CHAPTER 4 QUANTITATIVE EVALUATION OF MICROSTRUCTURAL CHANGES AND THEIR RELATIONS WITH SOME PHYSICAL CHARACTERISTICS OF FOOD DURING DRYING

In this chapter the results on the effect of hot air drying on the microstructural and some physical changes of carrot cubes are presented. In addition, the relationships between the microstructural and apparent physical changes (i.e., shrinkage and hardness) are discussed. Note that the microstructural changes were quantitatively investigated in terms of $\Delta FD/FD_0$ of microscopic images of the samples. $\overline{\Delta D} / \overline{D_0}$ and its distribution were also evaluated in relation to the apparent physical changes. This was done to compare whether $\Delta FD/FD_0$ of the microstructural images or $\overline{\Delta D} / \overline{D_0}$ is more influential on the apparent physical changes of the sample during hot air drying.

4.1 Drying Kinetics

The evolution of moisture content of carrot cubes undergoing hot air drying is represented in terms of the dimensionless moisture change (X/X_0) as shown in Figure 4.1. It is seen that the required drying time to reach the desired moisture content of around 0.1 kg/kg (d.b.) decreased with an increase in the drying temperature (420 min at 60 °C and 240 min at 80 °C). As expected, higher drying temperature led to a higher drying rate due to increased driving force for heat transfer, which is also related to the

rate of mass transfer. Moisture diffusivity is also higher at a higher drying temperature.

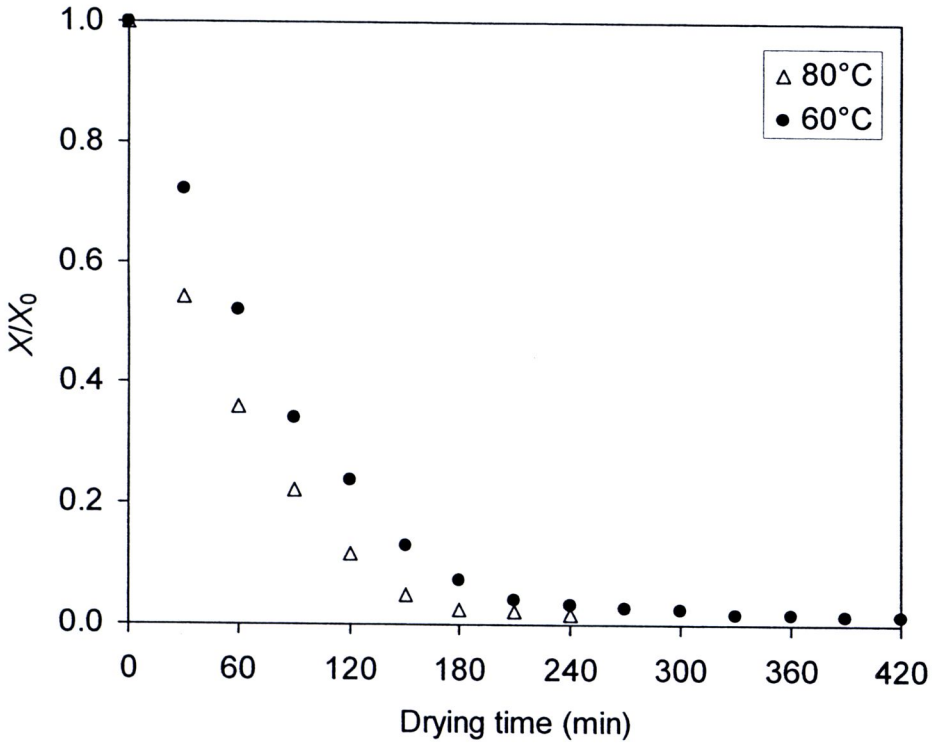

Figure 4.1 Hot air drying kinetics of carrot cubes

4.2 Microstructural Changes

As mentioned earlier in Section 3.6, SEM images were preferred over LM images in this study. It should be noted that based on the preliminary experiments it was found that the fractal dimensions of the SEM images were similar to those of the LM images. For example, at X/X_0 of around 0.02 (at drying time of around 180 min), $\Delta FD/FD_0$ of the LM images was in the range of 0.078 ± 0.002; $\Delta FD/FD_0$ of the SEM images was also 0.078 ± 0.005.

Figure 4.2 shows the relationships between $\overline{\Delta D} / \overline{D_0}$ as well as $\Delta FD/FD_0$ and the dimensionless moisture content of carrots undergoing hot air drying at 60 and 80 °C. The results showed that $\overline{\Delta D} / \overline{D_0}$ followed the same trend as that of $\Delta FD/FD_0$, i.e., both $\overline{\Delta D} / \overline{D_0}$ and $\Delta FD/FD_0$ increased with decreasing moisture content, indicating that the changes of the microstructure increased as the moisture content decreased. This is because water within the cells moved out during drying, leading the cells to be pulled down and collapsed. This resulted in a decrease in the cell dimension and less ordered structure occupied by cell walls and intercellular spaces. The trend of fractal dimension changes is in good agreement with that reported by Kerdpiboon and Devahastin (2007).

At higher moisture contents (X/X_0 of around 0.1-1.0), $\overline{\Delta D} / \overline{D_0}$ and $\Delta FD/FD_0$ increased almost linearly with a decrease in the moisture content, indicating that deformation of the cells as well as that of cell walls and intercellular spaces were proportional to the moisture loss. At lower moisture contents (X/X_0 of less than about 0.1), however, the changes of the moisture content were much slower than the changes of the microstructure. This is probably because at lower moisture contents the sample temperature approached the drying temperature, which was higher than the glass transition temperature of the sample (around 50 °C at moisture contents in the range of 0.1-0.2 kg/kg (d.b.); Georget et al., 1999). As a result, the sample suffered more structural collapse, leading to significant changes in the microstructure even when the moisture content did not change much (Rahman, 2001; Rahman, 2009; Mayor and Sereno, 2004).

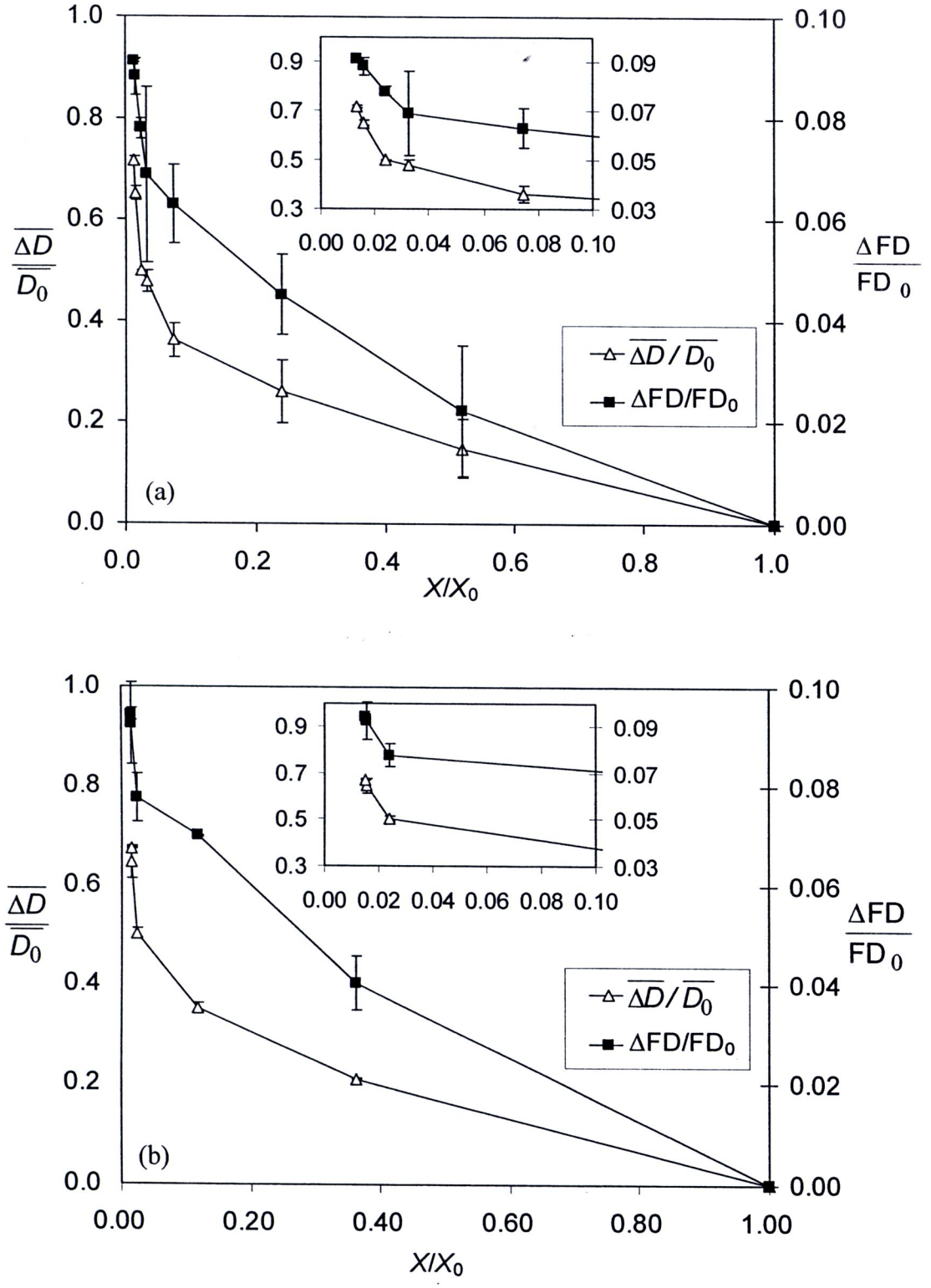

Figure 4.2 Relationships between $\overline{\Delta D}/\overline{D_0}$, $\Delta FD/FD_0$ and X/X_0 of carrot cubes undergoing hot air drying at (a) 60 °C; (b) 80 °C

The SEM photographs and corresponding cell diameter distributions are shown in Figures 4.3 and 4.4. It is noted that the average cell diameter of fresh carrots $\left(\overline{D_0}\right)$ was approximately 23-24 μm (Figures 4.3a and 4.4a), while the average cell diameter of dried carrots was about 5-7 μm (Figures 4.3e and 4.4e) toward the end of drying. Initially, the cells were approximately of a full round shape as shown in Figures 4.3a and 4.4a. During an early stage of drying moisture migrated from the cells to the sample surface. This led to a gradual decrease in the cell volume due to a rather uniform shrinkage of the cells as shown in Figures 4.3b and 4.4b, corresponding to a linear change in $\overline{\Delta D} / \overline{D_0}$ with a decrease in the moisture content (Figures 4.2a and 4.2b). This indicated that the deformation of the cells depended simply on the moisture loss. On the other hand, at lower moisture contents (X/X_0 equals to or less than about 0.1, see Figures 4.3c-e and 4.4c-e), non-uniform shrinkage and deformation of both cellular and other structures took place. The ruggedness of the cells increased, as expected. It was also observed that the cell diameter distribution curves gradually shifted toward smaller sizes in this period. The number of cells with larger diameters decreased as the moisture content decreased (Figures 4.3c-e and 4.4c-e). $\overline{\Delta D} / \overline{D_0}$ at X/X_0 of less than about 0.1 thus increased significantly, while X/X_0 did not change much (Figure 4.2).

It can also be seen in Figure 4.2 that the increased drying temperature (from 60 to 80 °C) caused larger changes of the fractal dimension, especially during an earlier period of drying, while $\overline{\Delta D} / \overline{D_0}$ was not much affected by the increased drying temperature. These results are supported by the SEM photographs in Figure 4.3 (for 60 °C) and Figure 4.4 (for 80 °C). At higher moisture contents (X/X_0 of around 0.1-1.0)

an increase in the drying temperature from 60 to 80 °C did not affect the change of the cell diameter. At the same X/X_0 the cell diameter distribution of a sample dried at 80°C was similar to that of a sample dried at 60 °C. This suggested that in an early period of drying the effect of drying temperature was not significant on $\overline{\Delta D} / \overline{D_0}$. In this early period cell walls and intercellular spaces of a sample was affected more by the increased drying temperature.

At the final stage of drying (X/X_0 less than 0.1) significant deformation of both cells and cell walls as well as intercellular spaces existed, whereas X/X_0 did not change much. As mentioned earlier, the deformation took place probably because the sample temperature approached the drying temperature and hence was higher than the glass transition temperature of the sample, leading to structural collapse (Rahman, 2001; Rahman, 2009; Mayor and Sereno, 2004). However, comparing the results at the same X/X_0, an increase in the drying temperature from 60 to 80 °C did not affect the deformation.

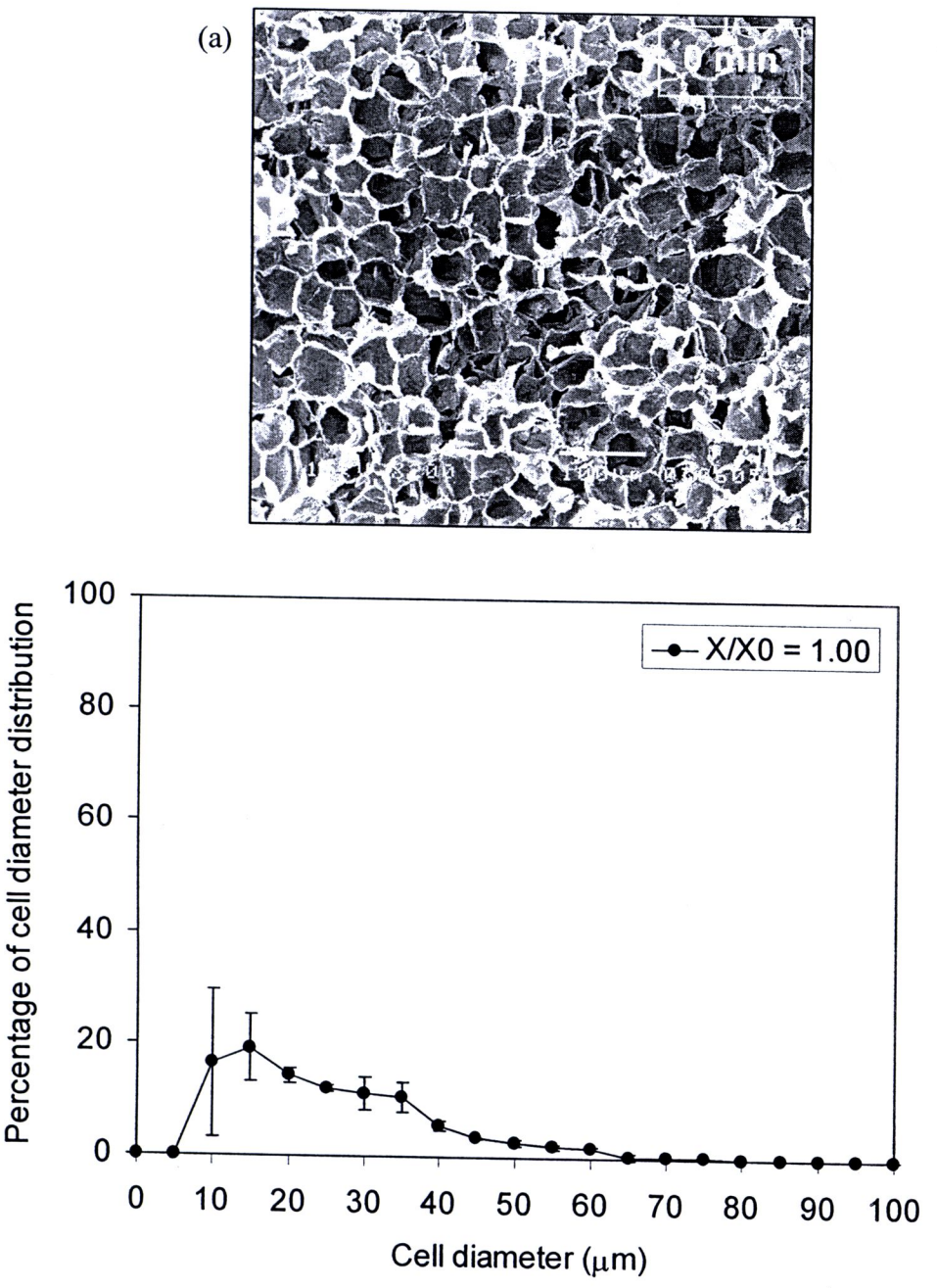

Figure 4.3 SEM photographs showing cross section of carrot cube undergoing hot air drying at 60 °C at (a) $X/X_0 \approx 1.00$; (b) $X/X_0 \approx 0.5$. Percentage of cell diameter distribution as a function of cell diameter of each microstructure is also shown.

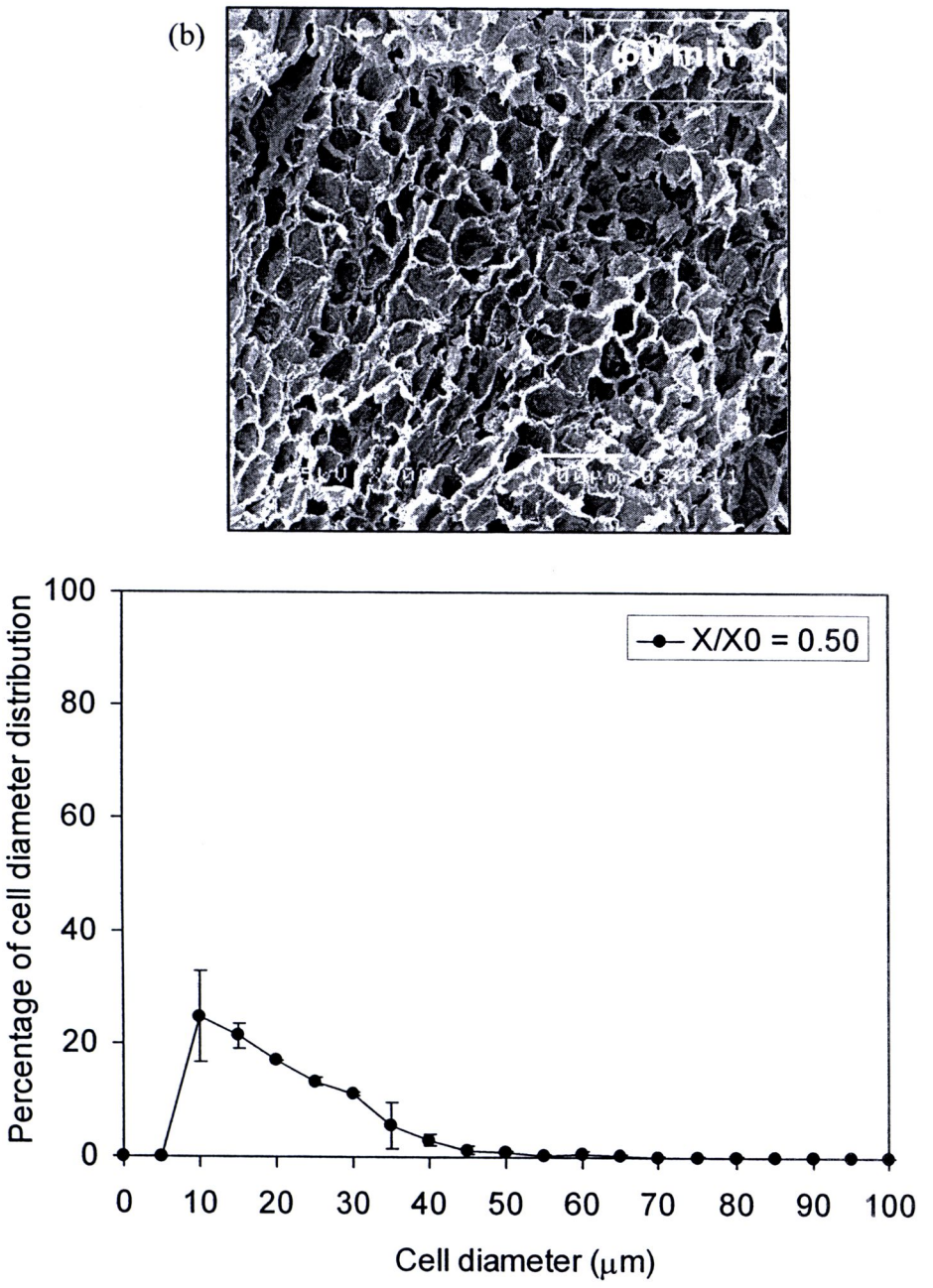

Figure 4.3 (cont'd) SEM photographs showing cross section of carrot cube undergoing hot air drying at 60 °C at (a) $X/X_0 \approx 1.00$; (b) $X/X_0 \approx 0.5$. Percentage of cell diameter distribution as a function of cell diameter of each microstructure is also shown.

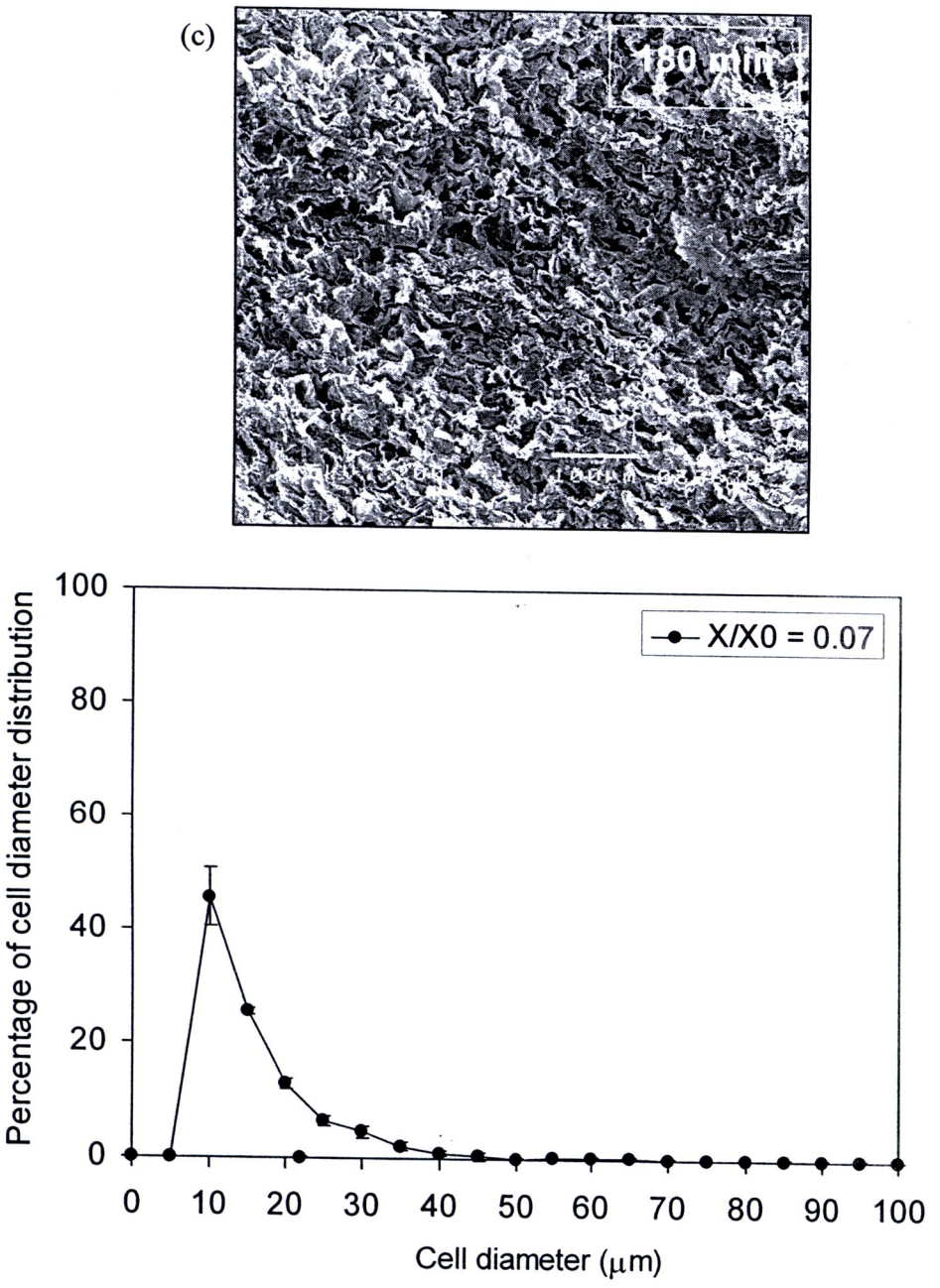

Figure 4.3 (cont'd) SEM photographs showing cross section of carrot cube undergoing hot air drying at 60 °C at (c) $X/X_0 \approx 0.1$; (d) $X/X_0 \approx 0.02$; (e) $X/X_0 \approx 0.01$. Percentage of cell diameter distribution as a function of cell diameter of each microstructure is also shown.

(d)

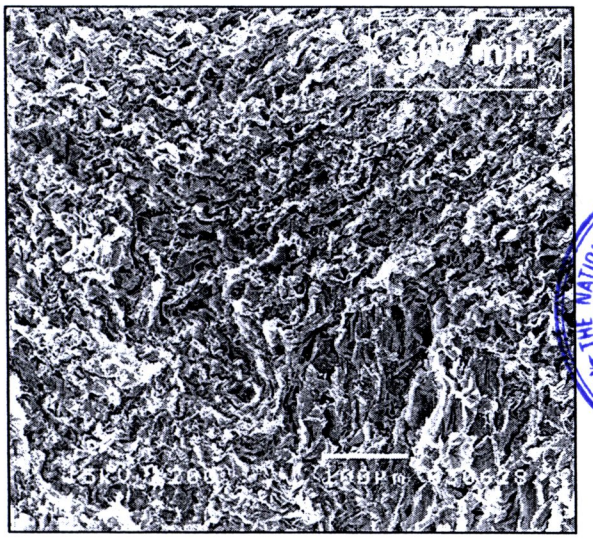

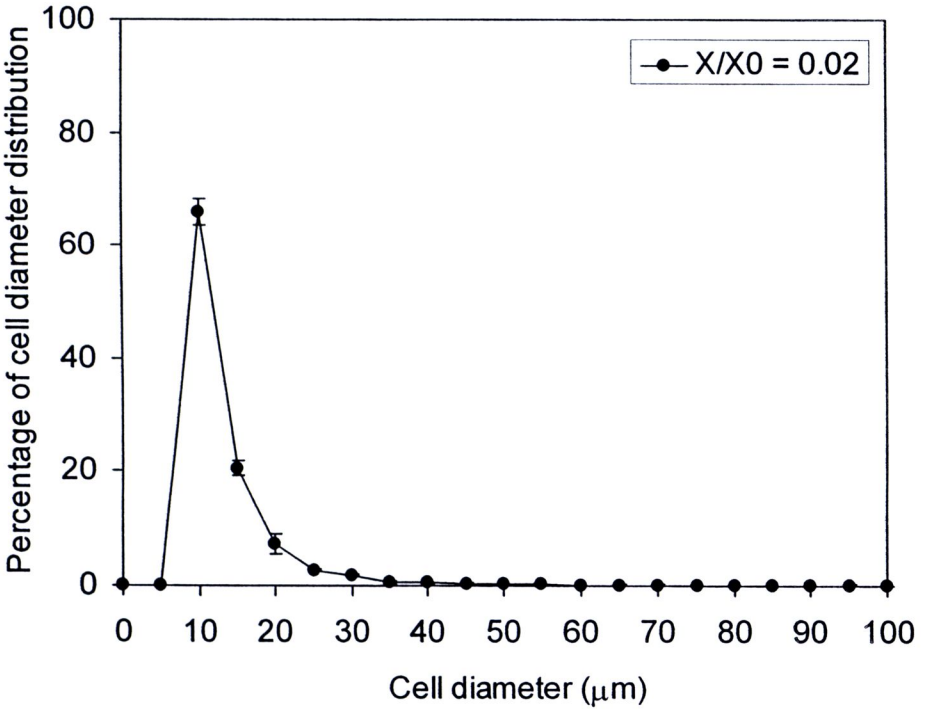

Figure 4.3 (cont'd) SEM photographs showing cross section of carrot cube undergoing hot air drying at 60 °C at (c) $X/X_0 \approx 0.1$; (d) $X/X_0 \approx 0.02$; (e) $X/X_0 \approx 0.01$. Percentage of cell diameter distribution as a function of cell diameter of each microstructure is also shown.

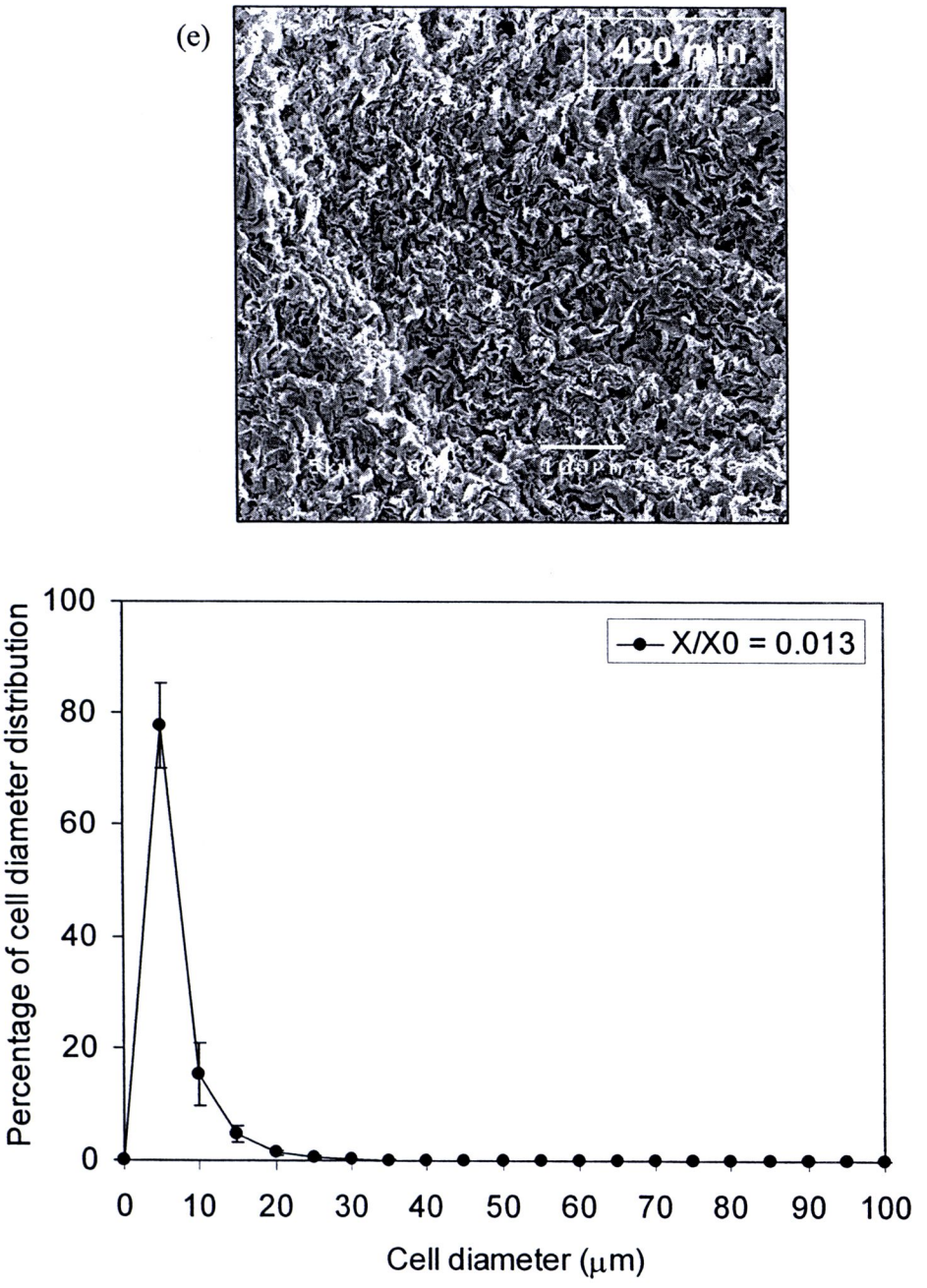

Figure 4.3 (cont'd) SEM photographs showing cross section of carrot cube undergoing hot air drying at 60 °C at (c) $X/X_0 \approx 0.1$; (d) $X/X_0 \approx 0.02$; (e) $X/X_0 \approx 0.01$. Percentage of cell diameter distribution as a function of cell diameter of each microstructure is also shown.

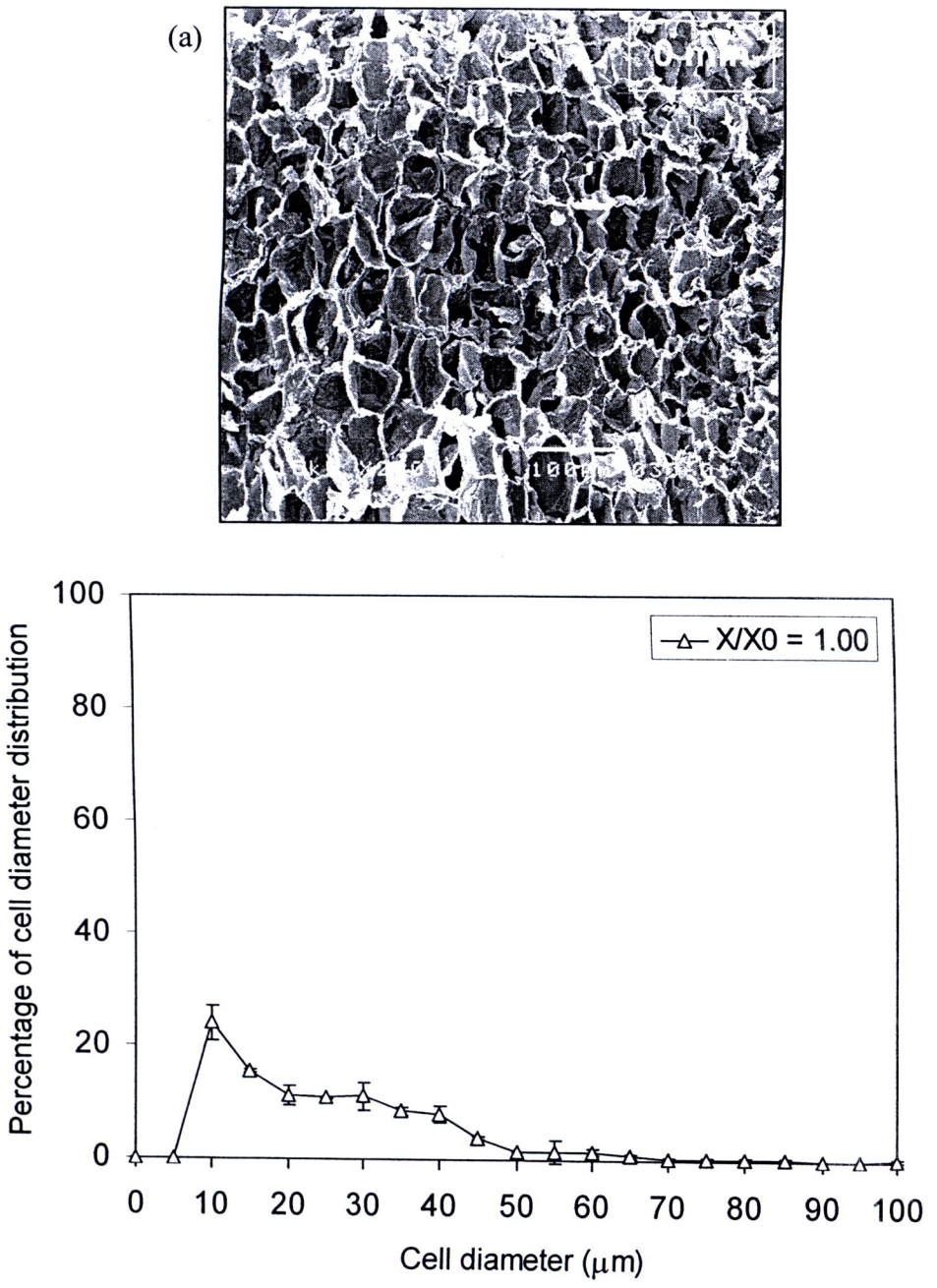

Figure 4.4 SEM photographs showing cross section of carrot cube undergoing hot air drying at 80 °C at (a) $X/X_0 \approx 1.0$; (b) $X/X_0 \approx 0.4$. Percentage of cell diameter distribution as a function of cell diameter of each microstructure is also shown.

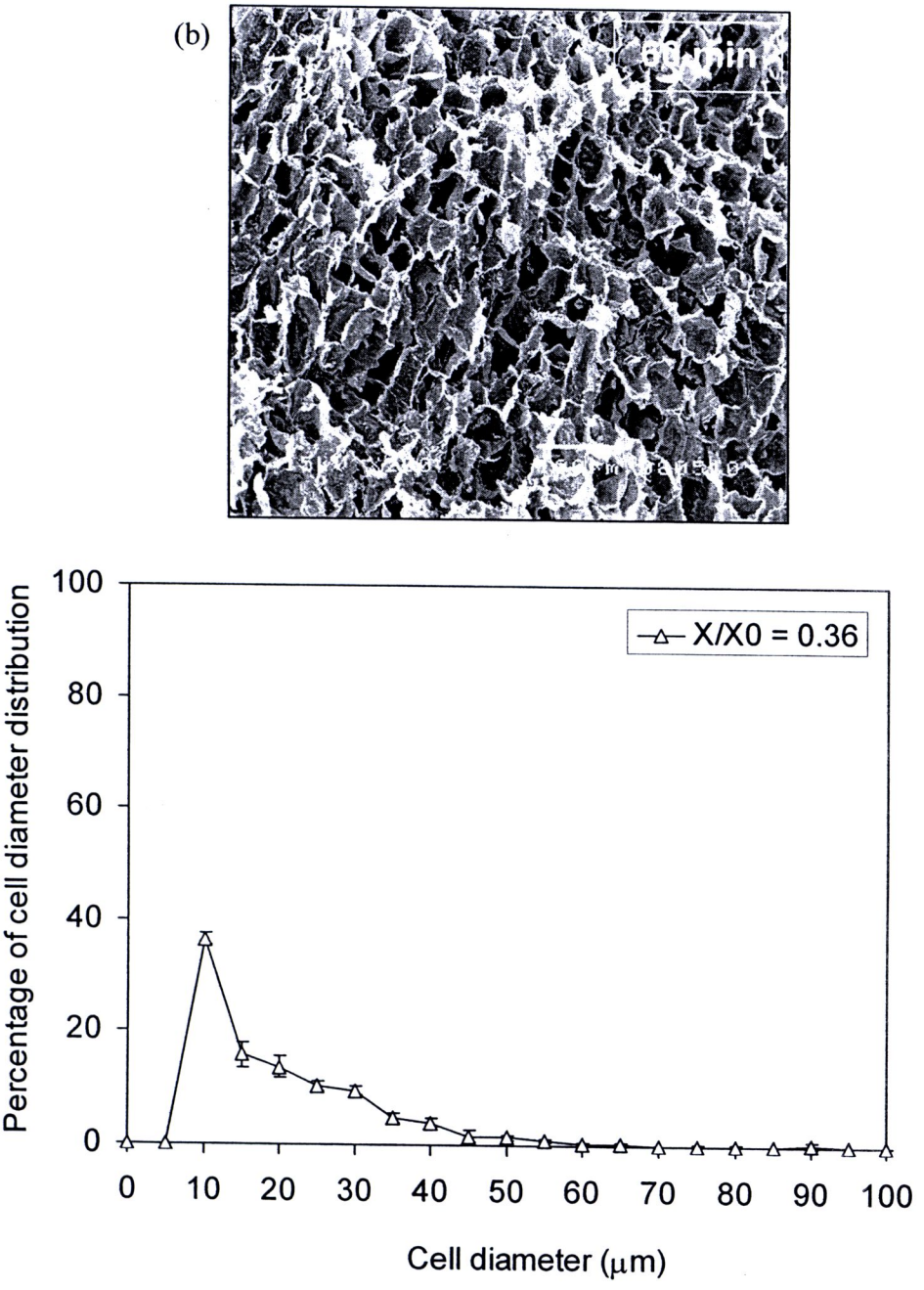

Figure 4.4 (cont'd) SEM photographs showing cross section of carrot cube undergoing hot air drying at 80 °C at (a) $X/X_0 \approx 1.0$; (b) $X/X_0 \approx 0.4$. Percentage of cell diameter distribution as a function of cell diameter of each microstructure is also shown.

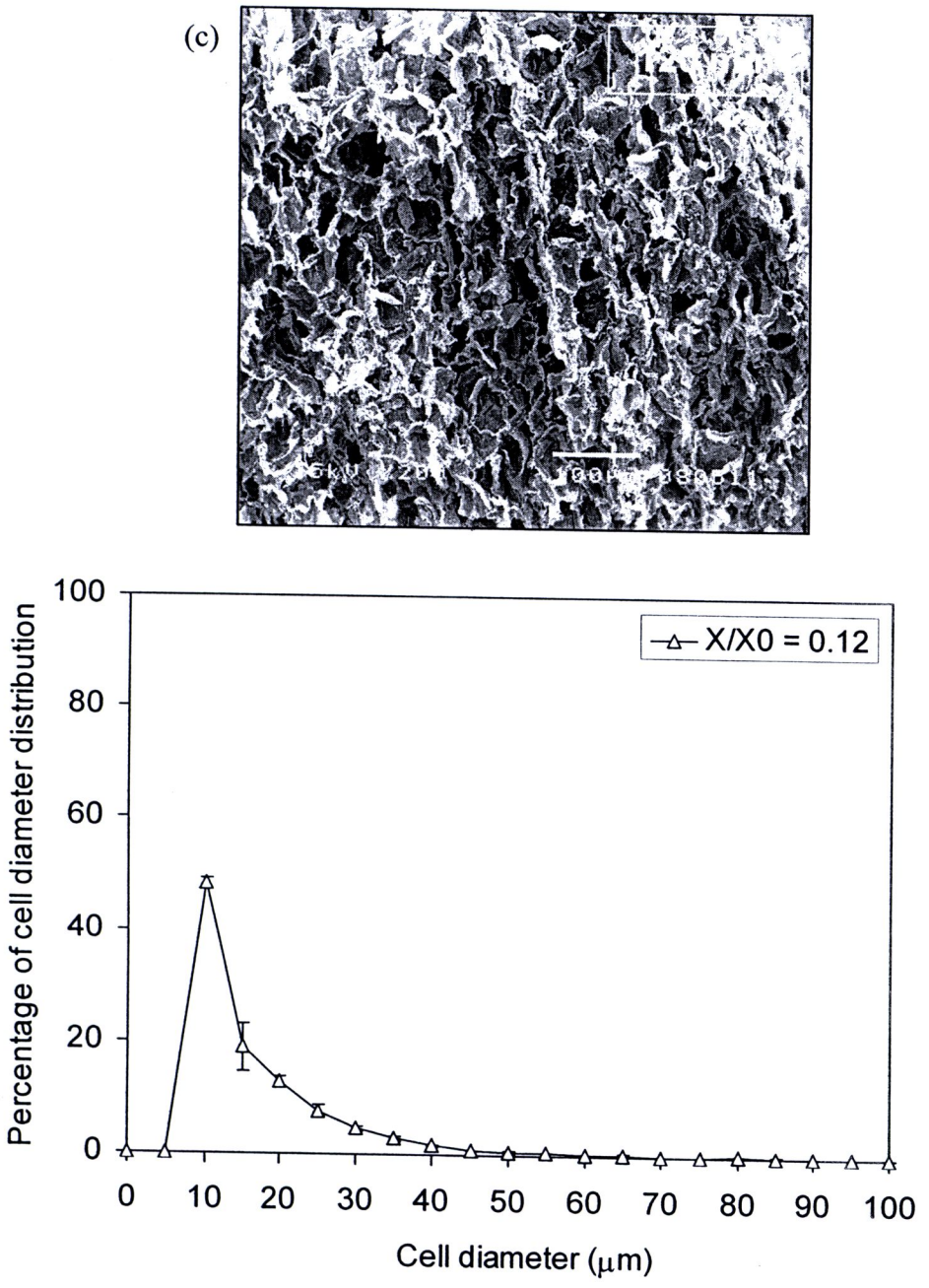

Figure 4.4 (cont'd) SEM photographs showing cross section of carrot cube undergoing hot air drying at 80 °C at (c) $X/X_0 \approx 0.1$; (d) $X/X_0 \approx 0.02$; (e) $X/X_0 \approx 0.01$. Percentage of cell diameter distribution as a function of cell diameter of each microstructure is also shown.

(d)

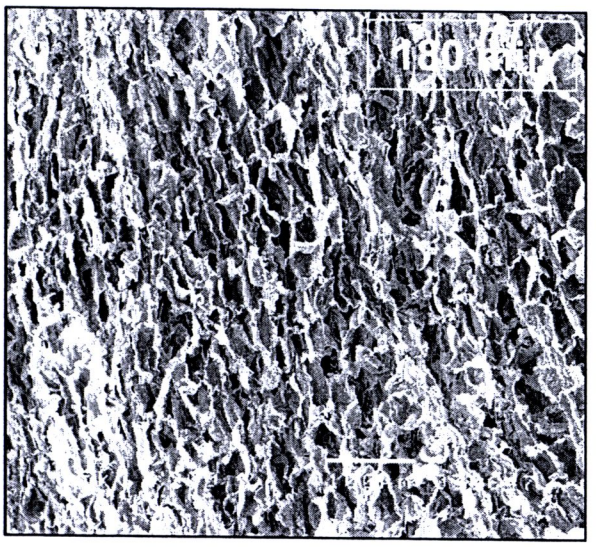

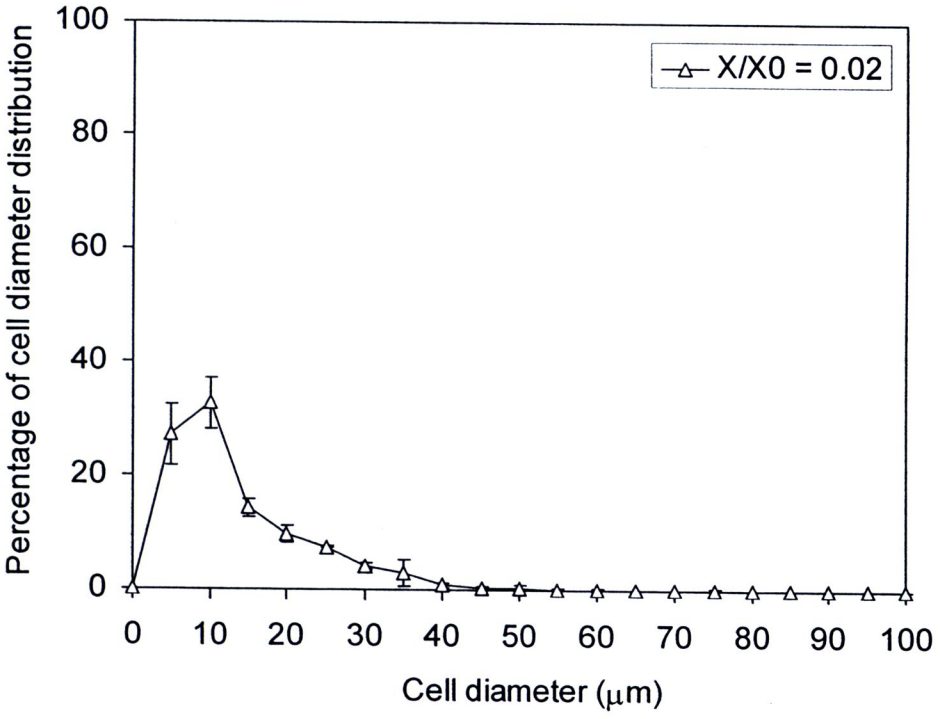

Figure 4.4 (cont'd) SEM photographs showing cross section of carrot cube undergoing hot air drying at 80 °C at (c) $X/X_0 \approx 0.1$; (d) $X/X_0 \approx 0.02$; (e) $X/X_0 \approx 0.01$. Percentage of cell diameter distribution as a function of cell diameter of each microstructure is also shown.

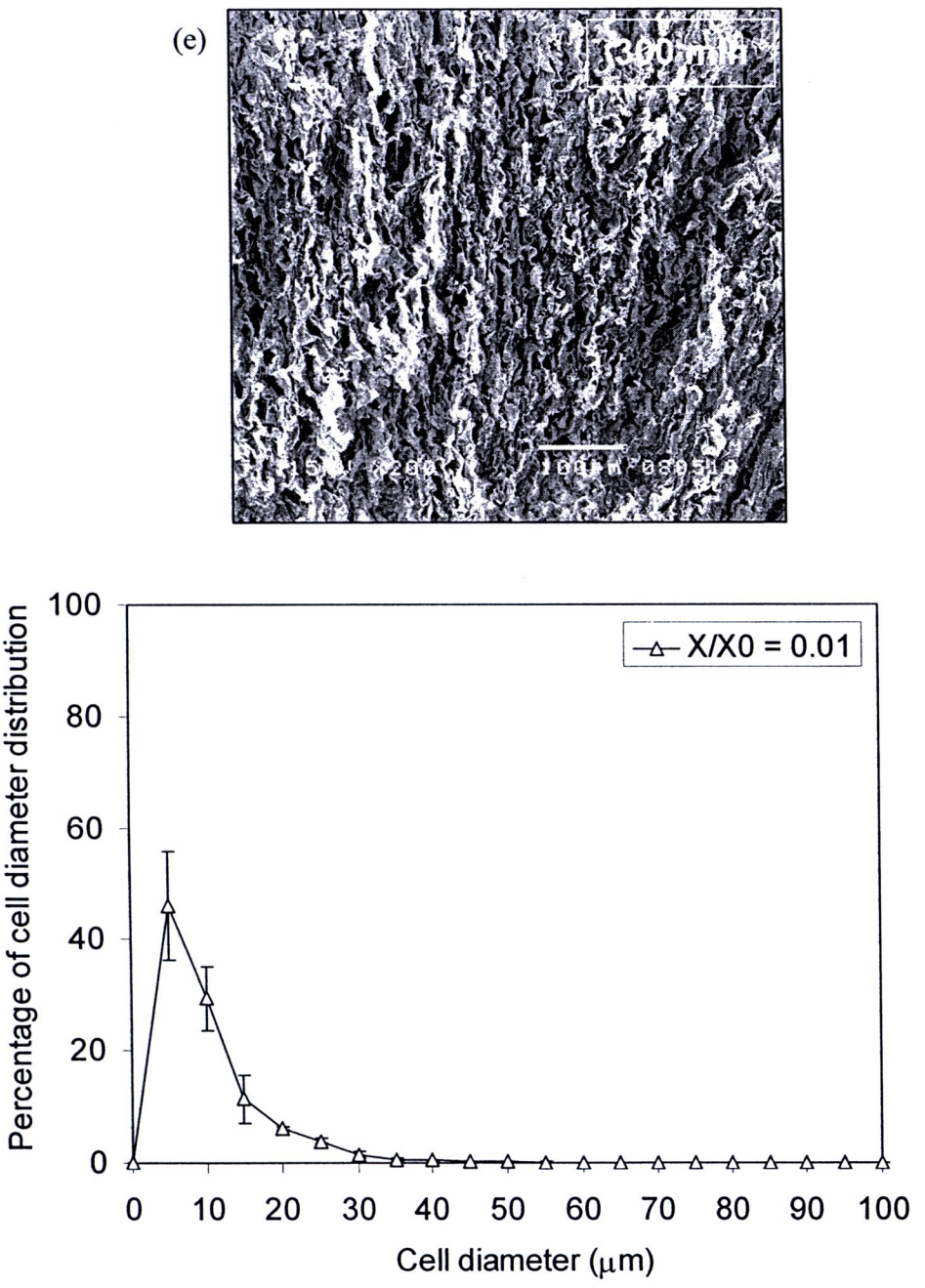

Figure 4.4 (cont'd) SEM photographs showing cross section of carrot cube undergoing hot air drying at 80 °C at (c) $X/X_0 \approx 0.1$; (d) $X/X_0 \approx 0.02$; (e) $X/X_0 \approx 0.01$. Percentage of cell diameter distribution as a function of cell diameter of each microstructure is also shown.

4.3 Relationships between Microstructural Changes and Physical Characteristics

The relationships between $\Delta FD/FD_0$ and the volumetric shrinkage of carrots undergoing hot air drying are shown in Figure 4.5a. It can be seen that the relationships between $\Delta FD/FD_0$ and volumetric shrinkage are quite well established. Nevertheless, it was observed that $\Delta FD/FD_0$ increased almost linearly with the shrinkage only up to a certain point (Figure 4.5a-A). At the final stage of drying, when the percentage of shrinkage reached around 80, $\Delta FD/FD_0$ started to change quite abruptly as shown in Figure 4.5a-B. This is probably because at low moisture contents a rigid crust or casehardening occurred; this retarded apparent dimension change (Ramos et al., 2004), but not the microstructure. Consequently, $\Delta FD/FD_0$ changed quite significantly, while the volumetric shrinkage (volume change) remained almost unchanged.

The relationship between $\overline{\Delta D} / \overline{D_0}$ and shrinkage (Figure 4.5b) followed a similar trend as that between $\Delta FD/FD_0$ and the volumetric shrinkage. Shrinkage developed no further when $\overline{\Delta D} / \overline{D_0}$ reached approximately 0.5. This point was the same as the point where $\Delta FD/FD_0 = 0.08$, at which the shrinkage started to be unchanged.

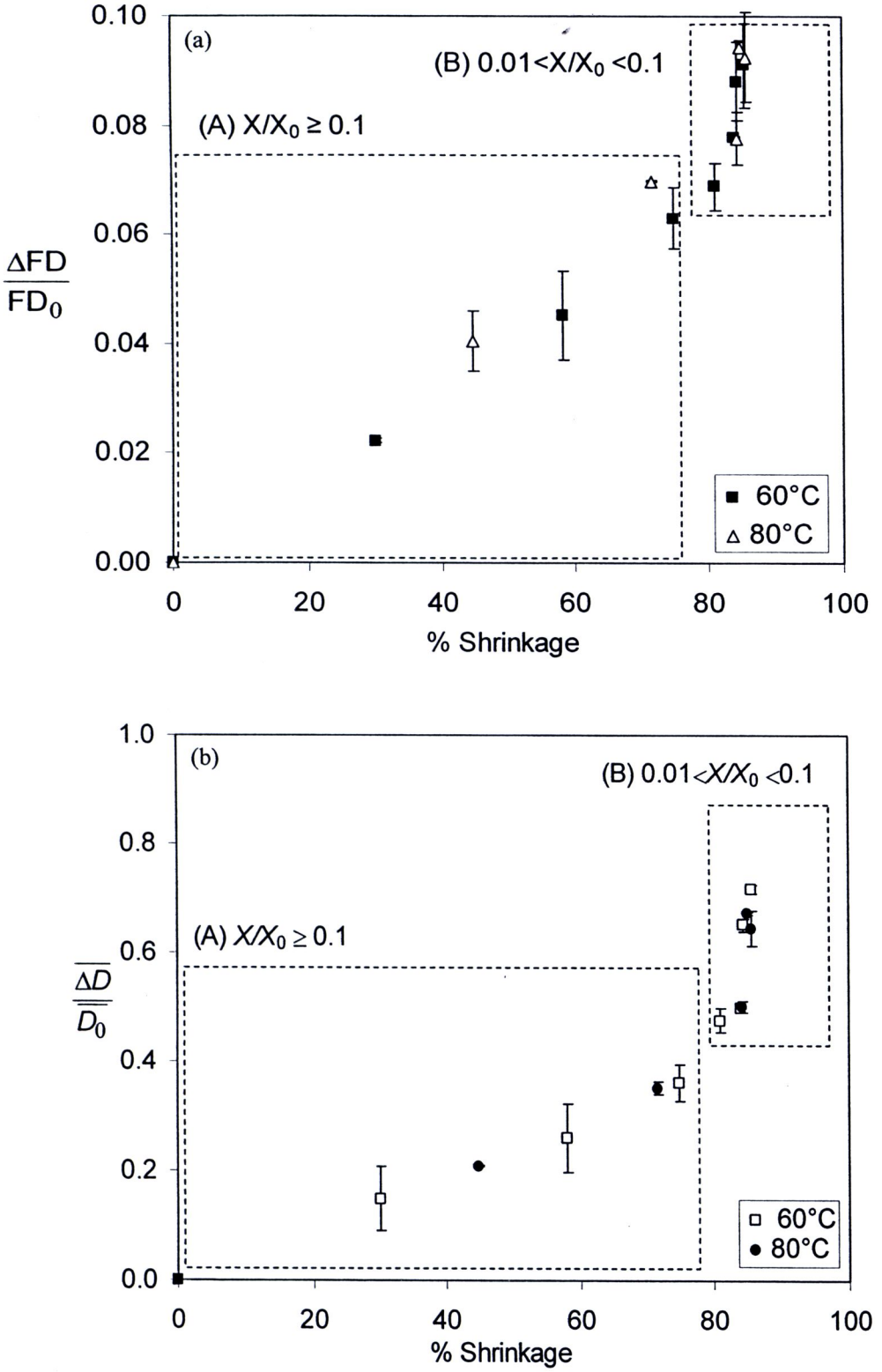

Figure 4.5 Relationships between microstructural changes and shrinkage of carrot cubes undergoing hot air drying at 60 and 80 °C

The hardness of carrot cubes undergoing hot air drying 60 and 80 °C is shown in Figure 4.6. It can be seen that the hardness tended to increase as the moisture content of the samples decreased. This in particular happened at lower moisture contents since the sample surface layers were rigid and crusted, while the cellular structure or the internal tissues might be ruptured, leading to higher mechanical resistance and hence higher values of hardness (Lewicki and Jakubczyk, 2004; Kowalski and Rybicki, 2007). Below $X/X_0 \approx 0.02$ the hardness increased suddenly. This is probably because the sample had undergone transformation from rubbery to leathery state. The sample was tough to deform (Rahman and Al-Farsi, 2005). Furthermore, the results showed that, at the same X/X_0, the hardness was not significantly affected by the different drying temperature.

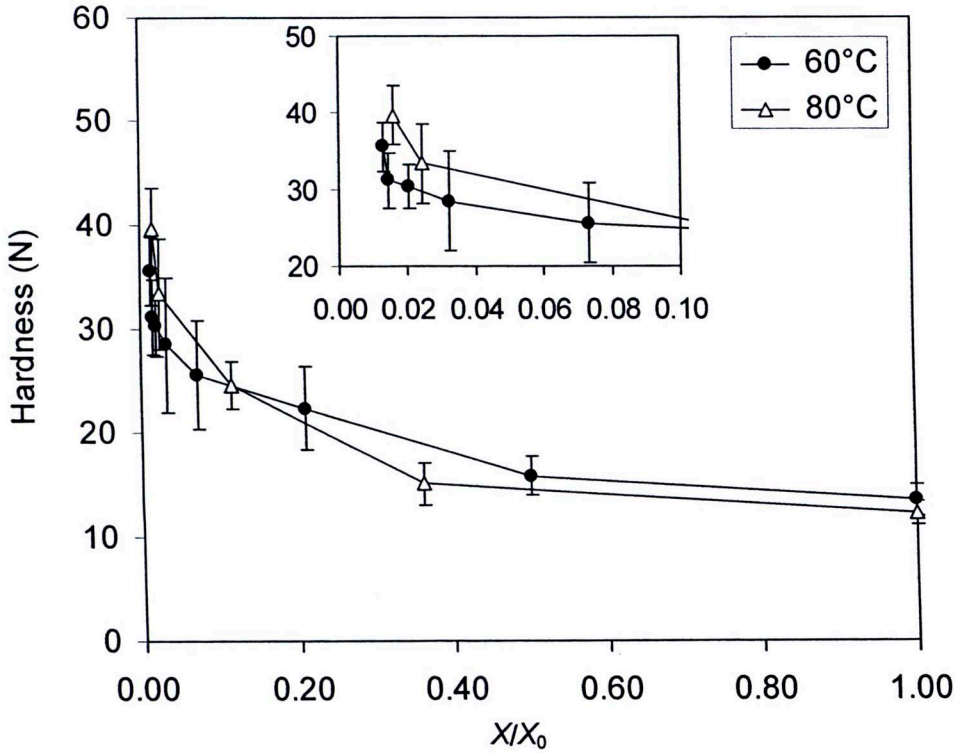

Figure 4.6 Hardness of carrot cubes undergoing hot air drying

The relationships between the microstructural changes ($\Delta FD/FD_0$ and $\overline{\Delta D}/\overline{D_0}$) and the hardness are shown in Figures 4.7a-b. It can be seen that $\Delta FD/FD_0$ and $\overline{\Delta D}/\overline{D_0}$ increased with an increase in the hardness. It was observed that there existed the proportional relationships between the microstructural changes and the hardness in all cases. This indicated that the changes in the cell wall and intercellular structure ($\Delta FD/FD_0$) as well as the cell diameter ($\overline{\Delta D}/\overline{D_0}$) (or, in other words, cellular structure) were the main factors that induced the hardness to increase during drying. It may thus be possible to say that either $\Delta FD/FD_0$ or $\overline{\Delta D}/\overline{D_0}$ could be used to monitor the hardness changes. For example, at $\Delta FD/FD_0$ and $\overline{\Delta D}/\overline{D_0}$ of around 0.06 and 0.4, respectively, the hardness of the samples was around 25-26 N in all cases.

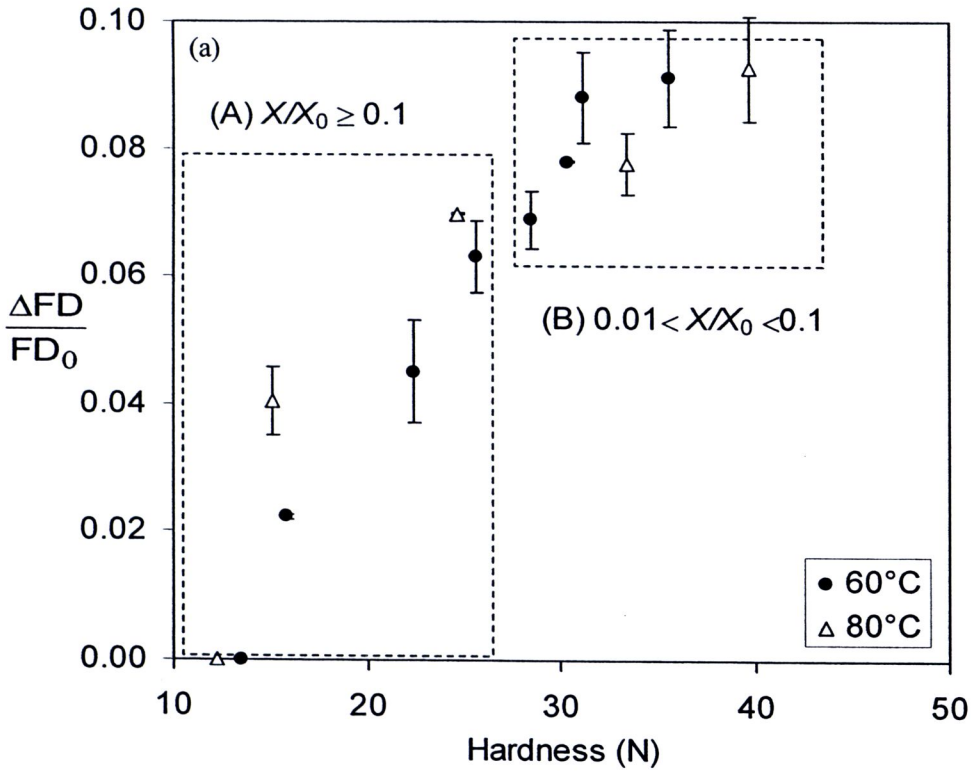

Figure 4.7 Relationships between microstructural changes and hardness of carrot cubes undergoing hot air drying at 60 and 80 °C

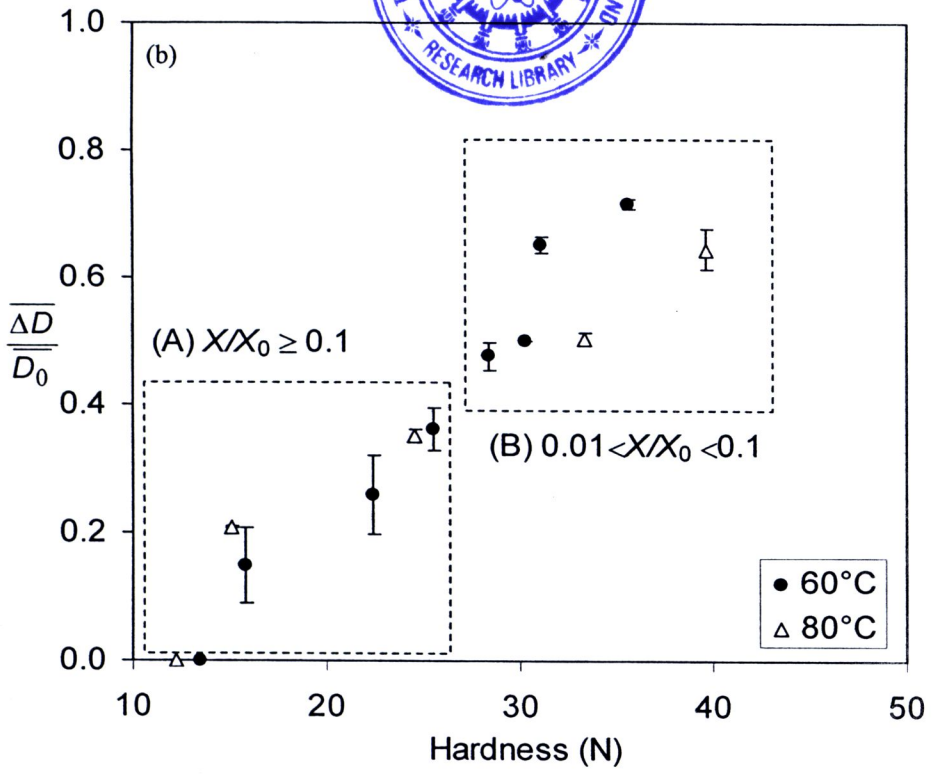

Figure 4.7 (cont'd) Relationships between microstructural changes and hardness of carrot cubes undergoing hot air drying at 60 and 80 °C

It was observed that the Pearson's correlation coefficients showed high level of relationships among $\Delta FD/FD_0$, $\overline{\Delta D}/\overline{D_0}$, shrinkage and hardness (Table 4.1). The results showed that both $\Delta FD/FD_0$ and $\overline{\Delta D}/\overline{D_0}$ correlated well with apparent physical changes; the Pearson's correlation coefficients representing $\Delta FD/FD_0$ and $\overline{\Delta D}/\overline{D_0}$ among apparent physical changes were between 0.84 and 0.98 depending on drying conditions.

Table 4.1 Pearson's correlation coefficients of various parameters

Condition		Parameter of interest				
		$\Delta FD/FD_0$	$\overline{\Delta D} / \overline{D_0}$	X/X_0	% Shrinkage	Hardness
60 °C	$\Delta FD/FD_0$	1.000	0.938	-0.946	0.950	0.957
	$\overline{\Delta D} / \overline{D_0}$		1.000	-0.836	0.857	0.966
	X/X_0			1.000	-0.992	-0.959
80 °C	$\Delta FD/FD_0$	1.000	0.968	-0.981	0.984	0.843
	$\overline{\Delta D} / \overline{D_0}$		1.000	-0.928	0.935	0.900
	X/X_0			1.000	-0.997	-0.983